



An Economical Tunable-Diode Laser Spectrometer for Fast-Response Measurements of Water Vapor in the Atmospheric Boundary Layer

Emily D. Wein¹, Lars E. Kalnajs², Darin W. Toohey¹

¹Department of Atmospheric and Oceanic Sciences, University of Colorado Boulder, Boulder, Colorado, USA

5 ²Laboratory for Atmospheric and Space Physics, University of Colorado Boulder, Boulder, Colorado, USA

Correspondence to: Emily Wein (Emily.wein@colorado.edu) and Darin Toohey (Toohey@colorado.edu)

Abstract.

The high spatiotemporal variability of water vapor in the atmospheric boundary layer possesses a significant measurement challenge with abundances varying by an order of magnitude over short spatial and temporal scales. Herein, we describe the design and characterization of an economical and flexible fast-response instrument for measurements of water vapor in the atmospheric boundary layer (ABL). The in-situ method of tunable-diode laser spectroscopy (TDLS) in the short-wave infrared (SWIR) was chosen based on a heritage with previous instruments developed in our laboratory and flown on research aircraft. The instrument is constructed from readily available components and based on low-cost distributed feedback laser diodes (DFB) that enjoy widespread use for high-speed fiber-optic telecommunications. A pair of versatile, high-speed ARM-based microcontrollers drive the laser and acquire and store data. High precision and reproducibility are obtained by tight temperature regulation of the laser via a miniature commercial proportional integrating (PI) controller. The instrument can be powered by two rechargeable 3.5 V lithium-ion batteries, consumes 2 W of power, weighs under 1 kg, and is comprised of hardware costing less than \$3,000. The new TDLS agrees within 2% compared to a laboratory standard and displays a precision of 10 ppm at a sample rate of 10 Hz. The new instrument allows users with little previous experience in instrumentation to acquire high quality, fast-response observations of water vapor for a variety of applications. These include frequent horizontal and vertical profiling by uncrewed aerial vehicles (UAVs), long-term eddy covariance measurements from fixed and portable flux towers, and routine measurements of humidity from weather stations in remote locations such as the polar ice caps, mountains, and glaciers.

1 Introduction

25 The sources, sinks, and transport of water vapor within the atmospheric boundary layer (ABL) are key components to radiation budgets and meteorology (Trenberth et al., 2005). Water vapor in the ABL displays high spatiotemporal variability due to the complex nature of land-surface interactions that drive sources (Santanello et al., 2018) and clouds and precipitation that drive sinks (Larson et al., 2002). At large scales, boundary layer water vapor mixing ratios vary from 1500 parts per million (ppm)



in the Arctic to 25,000 ppm in the Tropics, and they can range over five orders of magnitude from the surface to the upper
30 troposphere (Wulfmeyer et al., 2015). On scales of 100 to 1000 m, water vapor can vary by tens of percent because of
differences in local land surface, temperature dynamics and wind fields (Fischer et al., 2012; Kiemle et al., 2011; Shivers et
al., 2019). Observations of this variability are essential for elucidating the underlying mesoscale meteorological processes and
quantifying local-scale (100 m) radiation budgets (Fabry, 2006; Ogunjemiyo et al., 2002). Observations of the ABL and its
variability with high spatial and temporal resolution are necessary to resolve outstanding issues related to the prediction of
35 turbulent and convective processes and their impacts. However, observations have been limited by the relatively high cost of
existing instruments and lack of high quality data from more economical ones (Geerts et al., 2018).

Satellite-based remote sensing measurements are too coarse to resolve important variations of water vapor on very small
scales (Trent et al., 2018), therefore fast-response in situ and LIDAR-based instruments have become the primary methods for
observing water vapor from the surface and mobile platforms for process-oriented studies. The latter (e.g., DIALS and Raman
40 Lidars), capable of multidimensional measurements with spatiotemporal resolutions of 10 m to 100 m and greater than 1 s
(Wulfmeyer et al., 2015), are deployed frequently for profiling the ABL; however, their relatively high cost and operational
demands limit their usefulness for more widespread deployment. Alternatively, fast-response in situ instruments have found
increasing use in a variety of applications for measurements of small-scale variations in the ABL capturing the smallest and
fastest atmospheric variations near the surface where the atmosphere is not well mixed (Geerts et al., 2018). Incorporating high
45 sampling rates faster than 1 Hz, instruments such as the infrared gas analyzers (IRGAs) that rely on non-dispersive infrared
light have come to routinely monitor surface-based fluxes of H₂O and CO₂ within ecosystems (Aubinet et al., 2012). To date
these instruments, tend to be highly specialized and available from a small number of vendors as research-grade tools for
observations from weather stations or flux towers. In addition, they typically cost \$20,000 or more and they require frequent
maintenance and calibration from the original factory.

50 At the other end of the cost spectrum are various versions of capacitive humidity sensors that have found frequent use
among hobbyists and research scientists for routine measurements from surface weather stations (Muller et al., 2015). These
tiny sensors, costing only tens to hundreds of dollars, employ thin-film water-sensitive polymers sandwiched between two
electrodes. They have been used in radiosondes for more than 40 years, and they can be accurate to ~0.8 % over a wide range
of humidities. Although they are small and relatively inexpensive, they respond slowly to changes in water vapor, and they
55 exhibit measurement biases that limit their usefulness for high-frequency observations (e.g. Miloshevich et al., 2009, 2004;
Segales et al., 2022).

As fast in situ observations of H₂O are essential for numerical weather predictions and for investigations of the evolution
of the ABL and its turbulence characteristics (e.g. large eddy simulations) (Petersen, 2016; Helbig et al., 2021), a more
economical instrument for fast, high-accuracy measurements of water vapor in the ABL is desirable. Here, we report on the
60 performance of a new, tunable-diode laser spectrometer (TDLS) capable of fast-response measurements of water vapor in the
ABL. Demonstrating high accuracy/precision like research-grade commercial instruments, yet exhibiting low cost and
flexibility desired for more routine observations, the instrument bridges the gap between the more expensive, highly accurate



fast-response instruments and the relatively inexpensive, but slower response capacitive instruments. The design is an adaptation of previous TDLS instruments that have a 30-year history of use on research aircraft including the NASA ER-2
65 (May, 1998; May and Webster, 1993), DC-8 (Hallar et al., 2004; Newell et al., 1996), WB-57F (Davis et al., 2007) and NCAR
GV (Dorsi et al., 2014). As in a previous design (Dorsi et al., 2014), it employs a commercial telecommunications fiber-
coupled distributed feedback (DFB) laser in a generic package with self-contained thermoelectric coolers (TEC) for precise
selection of wavelength and to reduce artifacts due to absorption by water vapor in trapped spaces in complex coupling optics.
The instrument is built from commercial, off-the-shelf technology, and it exhibits performance comparable to instruments
70 costing orders of magnitude more. The new design is flexible and simple, allowing for accurate and reliable measurements of
water vapor for investigators with little previous experience with research grade instruments, while being easily adaptable to
different contexts and other atmospheric species.

Several immediate applications are envisioned for this new instrument. One involves fast-response, open-path
observations of water vapor from a small uncrewed aerial vehicle (UAV) such as a hexacopter. While this application has
75 already been explored (e.g. Bärfuss et al., 2023; Pillar-Little et al., 2021; Segales et al., 2020; Varentsov et al., 2023) the
available instrumentation have slow response and limited vertical resolution (Segales et al., 2022). The instrument described
in this paper would be ideal for obtaining observations over very small scales (e.g., centimeters), including obtaining frequent
high-resolution thermodynamic profiles at locations where observational gaps limit numerical weather prediction and climate
modelling (Kämpfer, 2013). Another application is tracking water-resource loss from reservoirs with ground-based flux
80 measurements. There is a need to increase the density of measurements on specific reservoirs to map out the effect of terrain
and variable field inhomogeneity (Friedrich et al., 2018). Expanding sensor networks with an economical instrument that
maintains high accuracy and precision to monitor evaporation in regions of complex terrain where there is a need for
simultaneous observations can open up new areas of study and fill gaps where there is limited knowledge of the importance of
evaporation to water availability, especially in arid regions (Roth and Blanken, 2023). Such a capability will also enable new
85 studies of ecosystem exchange in geographic regions that have been historically underserved, for example in developing
countries (Markwitz and Siebicke, 2019; Kim et al., 2022).

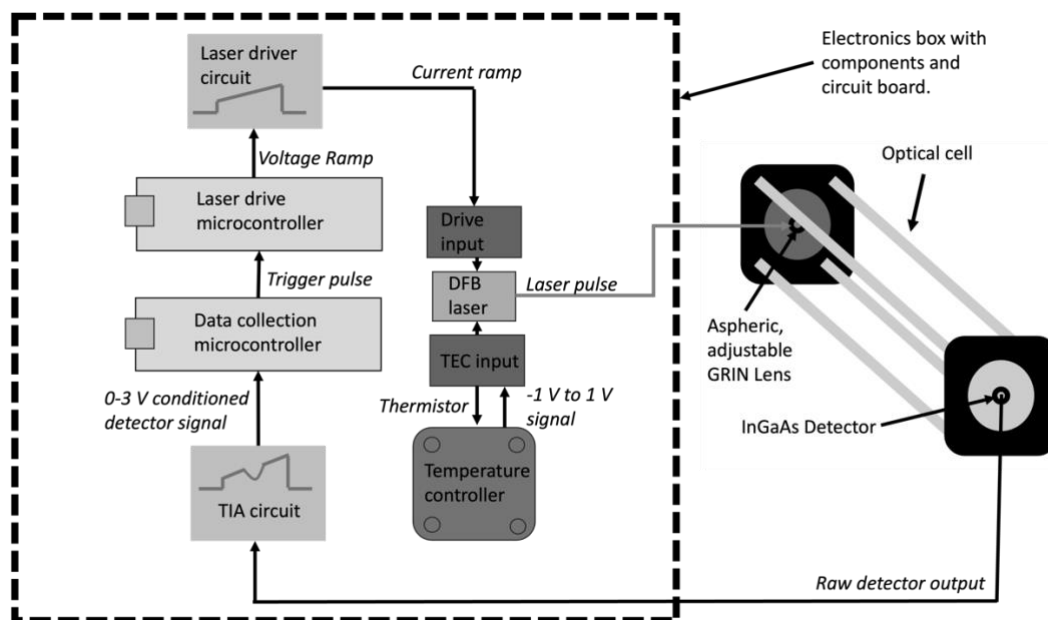
2 Instrument Design

2.1 Hardware Description

The TDLS instrument described here is based off a design reported previously for measurements of condensed water
90 contents from research aircraft (Dorsi et al., 2014); a schematic of which is shown in Fig. 1. A DFB laser diode emitting
radiation with a wavelength centered at 1368.6 nm at room temperature (NLK1E56AA, NTT Innovative Devices, Yokohama,
Japan) rapidly scans over a strong water vapor absorption line. To avoid damping of high-frequency variations a short (~20
cm), open-path, single-pass optical cell was constructed of low-cost commercial components. Water vapor mixing ratios in the
range 2000-20,000 ppm are readily retrieved with high precision (+/- 10 ppm). The primary novelty of the new TDLS is a low-



95 power, low-cost electronics package that simultaneously drives the laser with rapid linear current ramps over a highly stable wavelength range while acquiring data for subsequent processing of the scans into accurate mixing ratios based on laboratory calibrations.



100

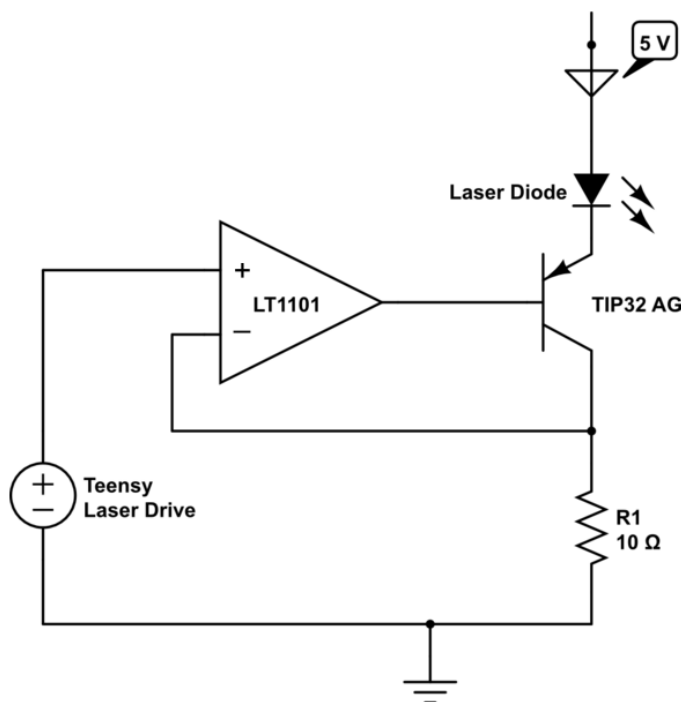
Figure 1. Schematic diagram of the new TDLS. Arrows represent direction of information flow between components.

The laser temperature is tuned to the wavelength of a strong water absorption feature centered at 1368.59 nm with a commercial proportional-integral (PI) controller (WTC 3243, Wavelength Electronics, Bozeman, MT). (Gordon et al., 2022).
105 A highly stable temperature of 0.002 K, consistent with the manufacturer’s specification, is maintained with a fixed set point from a voltage divider sourced with a high-precision reference (e.g., LDLN025M25R, STMicroelectronics, Geneva, Switzerland) and a variable resistor. This stability is important for maintaining a reproducible output wavelength of the DFB. If desired, a voltage from the digital-to-analog (DAC) output from one of the microcontrollers can also be used for dynamic temperature control.

110 Two Teensy Arduino compatible microcontrollers are chosen for the laser-driving (“driver”) and data-acquisition (“receiver) functions. These microcontrollers are based off low-cost ARM RISC Cortex-M processors, exhibiting a balance of speed and configurability. Previous instruments employed single or multi-core general purpose processors running full operating systems such as Linux on a PC-104 form factor single board computer (e.g Hallar et al., 2004; Dorsi et al., 2014). Unpublished work in our lab (Rainwater, 2022) showed that imprecise timing of the output ramp for the laser caused by
115 software interrupts produced unstable PI temperature of the DFB TEC that result in wavelength “jitter” (movement of the



position of the line center in the laser scan). Separating the input and output functions allows for precise control of the laser and highly reproducible scans to ~10 kHz and faster, resulting in high precision of the measurements. The microcontrollers simplify the electronics while also allowing for uninterrupted laser scanning while the detector signal is acquired, processed, and stored.



120

Figure 2. Schematic figure for the laser drive circuit described below. The individual components used in this instrument are labeled. R1 requires a resistor with a high current tolerance with the current pulled through the transistor contingent on the value of R1 and max voltage output of the Teensy drive.

125

A Teensy 3.6 with integrated 12-bit, 10^6 samples per second DAC provides the drive voltage for scanning the DFB current. Prior to the start of each scan, the laser driver produces a pulse (“trigger”), shown on the bottom panel of Fig. 3, on a separate digital line that initiates the data acquisition and storage process on the receiver. The current required to scan the laser is produced by passing the DAC output from the Teensy 3.6 through a custom-built voltage-to-current operational amplifier with the laser diode biased by 5 V. The scan rate, range, and repetition rate period are configured in software. Teensy model 4.1 was used for data acquisition and storage with a built in Micro-SD card feature. Upon receiving the trigger pulse, the internal clock is recorded into a buffer and the ADC is started. The top panel in Fig. 3 shows the acquired detector output consisting of 445 discrete points (7.2 kHz raw ADC rate) sampled at 12-bit resolution, oversampled 32 times using a built-in averaging function to reduce noise inherent in the Teensy. This results in a minimum resolvable signal of ~0.2 mV. The middle

130



135 V. panel in Fig. 3 shows an example of a series of linear ramps, each consisting of 1366 discrete one-bit steps from 0.80 V to 1.9

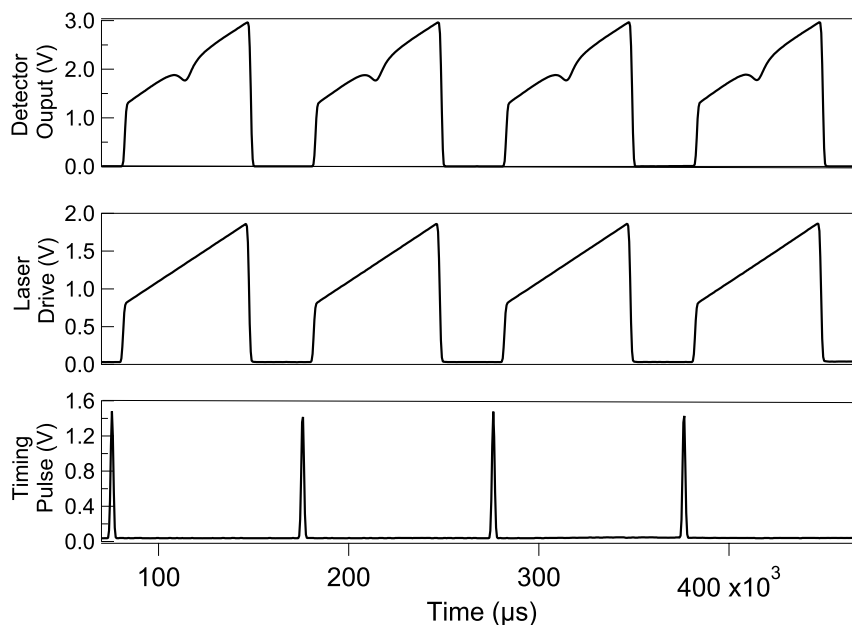


Figure 3. Important components of the TDLs laser scans as a function of time. Detector signal (top panel), laser drive voltage (middle panel), and trigger pulse signal (bottom panel). See text for explanation.

140 For this work, a single pass, open-path, 21.5 cm optical cell was constructed with a fixed 30-mm cage plate assembly (Thorlabs, Newton, NJ). One end housed an adjustable aspheric collimating lens (CFC11A-C Adjustable Fiber Collimator, FC/APC, $f = 11.0$ mm, 1050 - 1620 nm AR, Thorlabs, Newton, NJ) that was attached to the FC/APC output of the DFB laser, the divergence of which was opened to fully illuminate the active area of a low-noise broadband indium gallium arsenide (InGaAs) semiconductor photodiode (either Thorlabs FDGA05 or Fermionics FD1500) on the opposite side of optical path
145 both operated in photovoltaic mode. Intensity variations due to vibration and turbulent fluctuations of air density in the optical path are minimized as the beam width is larger than the active area of the photodiode. The photodiode is operated in photovoltaic mode and the photocurrent is converted to a voltage up to a maximum of 3.3 V with a custom-built low-noise transimpedance amplifier circuit using a single-supply operational amplifier amp (AD1101, Analog Devices, Wilmington, MA). The gain could be tuned using a variable resistor, was adjustable with a 1-10 k Ω variable resistor.

150 The two microcontrollers, laser temperature controller, detector amplifier, batteries, and power conditioning were placed on a custom-built circuit board (OSHPark, Portland, OR). The instrument is powered on or off with a single-pole-single-throw toggle switch, with a small light-emitting diode (LED) that indicates when the instrument is running. An LED on the receiver Teensy indicates when data are being written to the MicroSD card. The entire system consumes 2.5 W, and it can operate for 2 h when powered by two 3.6 V rechargeable lithium-ion batteries (e.g., ARB-L16-700UP, Fenix Lighting, Littleton, CO).



155 Alternatively, the instrument can be run indefinitely via 5 V passed through the Teensy microUSB input. All components, except the optical cell and coupling laser fiber-optic cable and twisted-pair electrical wires to the detector, can fit in a box with dimensions of 16.18 x 11.18 x 4.90 cm (PN-1324-C, Solutions Direct, Riverside, CA), with the laser output fiber and twisted pair of wires from the detector passing through a hermetic seal.

160 2.2 Spectral Processing

Water vapor concentrations are derived using the approach described previously (Dorsi et al., 2014). Figure 4a shows a single scan over the absorption line consisting of 445 individual measurements of the amplified detector signal. Briefly, a small detector/amplifier offset is determined from 30 points at the start and 20 from the end of each scan while the laser is powered off. Then, linear segments near the beginning and end of the linear current ramp outside of the water vapor absorption feature are identified for calculating background (i.e., $I_0(t)$) based on a 1st-order polynomial fit (dashed line in Fig. 4a). Scan step number (or elapsed time) is converted to wavelength based on an empirical function derived by using the spacing of line centers of a pair of water absorption lines as a ruler when mapping the laser tune range as a function of laser TEC temperature. This is convenient as it accounts for the possible drift of the tune temperature by removing the nonlinear output laser wavelength in response to a linear current ramp and allowed us to determine the width of the scan to be 0.279 nm. The observed signal (i.e., $I_{\text{obs}}(t)$) and calculated background $I_0(t)$ are then placed in an array $[\lambda_i, I_o(\lambda_i), I(\lambda_i)]$. Based on the Beer-Lambert Law, water concentration is proportional to the integral of absorbance $A = \ln(I_o/I)$ over the full width of the absorption line. This integral is estimated as the sum of discrete points as in Eq. (1).

$$\int A(\lambda) d\lambda = \sum_{k=1}^{385} A(\lambda)_k * \Delta\lambda_k \quad (1)$$

175

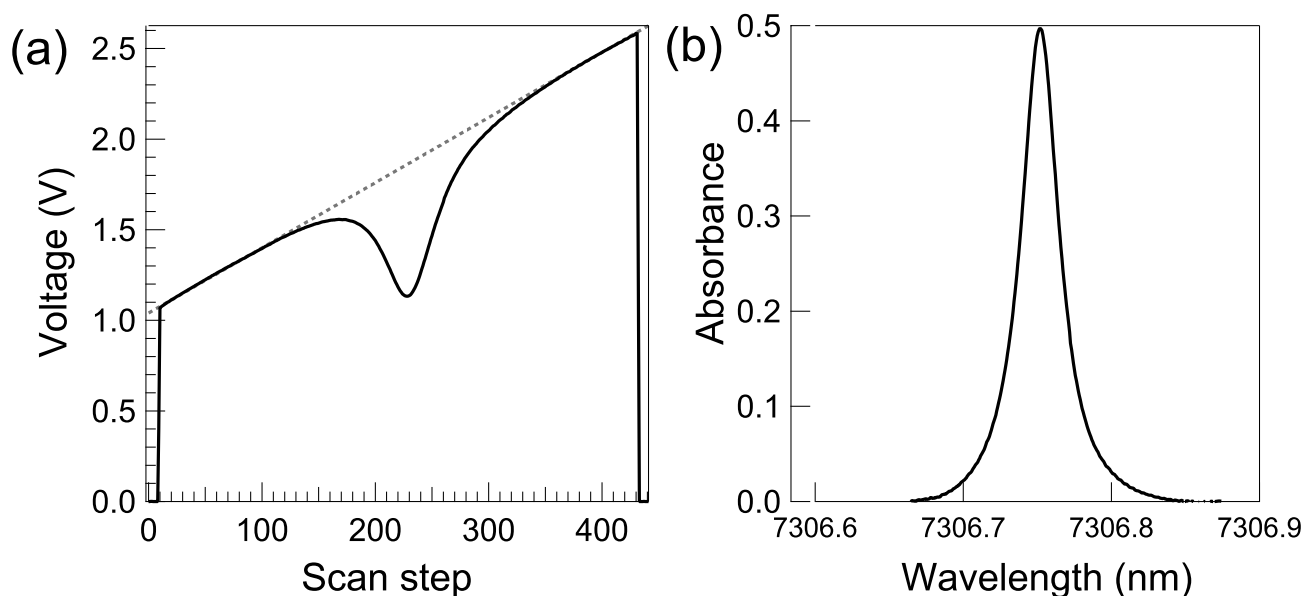
An example of a single laser scan converted to absorbance is shown in Fig. 4b. The resulting integral is related to concentration of water vapor by a response factor determined by laboratory calibration using a high-accuracy cavity ringdown spectrometer, CRDS (L-2120i, Picarro, Santa Clara, CA), referenced to a dew-point generator (LI-610, LiCor, Lincoln, NE) (Noone et al., 2011; Henze et al., 2023). Ambient water concentrations and mixing ratios are interchangeable through the Ideal Gas Law using concurrent measurements of temperature and pressure, which, for this work, were measured with a small sensor (BMP280, Bosch Sensortec, Reutlingen, Germany) placed midway between the output lens of the laser and the detector just outside the laser beam. The precision of this sensor was measured to be +/-1 Pa and +/-0.01° C.

For this work, we store the raw scan data with T, P and a timestamp and perform data analysis in post processing using code written in Python. This maximizes precision and flexibility while allowing us to evaluate performance with various diagnostic variables (e.g. those investigating stability or interference) that are only derivable from raw scans. Future iterations of this design will be simplified to include real time processing of the spectra on the Teensy 4.1 before data are written on the microSD card. These calculations take a fraction of the clock cycles needed for writing an entire raw scan so don't affect

185



instrument time response. In the meantime, we have uploaded our Arduino sketches and processing codes to GitHub opensource.



190

Figure 4. (a) Example of the output of the transimpedance amplifier for a single scan of the DFB laser consisting of 445 discrete points. The initial ~10 points and final ~10 points represent the signal with the laser powered off. The dashed line is a linear fit in a region where absorbance by H₂O is negligible (defined as I_0). (b) Absorbance defined as $\ln(I_0/I)$ for a single scan of the DFB laser shown in Fig. 3. Wavelength is determined as described in the text.

195

3 Results

The TDLS integrals were calibrated by sampling a series of mixing ratios spanning the range 5,000 ppm to 27,000 ppm in a 250-L Polycarbonate chamber alongside the CRDS. The TDLS optical cell was placed in the center of the chamber, and a fan was used to assure the chamber was well mixed. The sampling line of the CRDS was aligned with the mid-point of the TDLS open-path cell and positioned just outside the path of the laser beam. The chamber was first saturated to a mixing ratio of ~27,000 ppm with the dew point generator, after which lab air with ~13,000 ppm of H₂O was admitted to the chamber stepwise approximately every five minutes over the course of several hours. Thus, a series of values spanning the range 13,000 ppm to 27,000 ppm was obtained. Values lower than 13,000 ppm were produced by further dilutions using a flow of dry air from a cylinder of Ultra Zero Air (H₂O < 2 ppm, total hydrocarbons < 0.1 ppm, Airgas, Dacono, CO). TDLS concentrations were converted to mixing ratios using pressure and temperature as measured from the BMP280 sensor, and the results are shown in Fig. 5. The deviation between the two data sets is less than 2 % over the range 5000 ppm to 25,000 ppm.

205

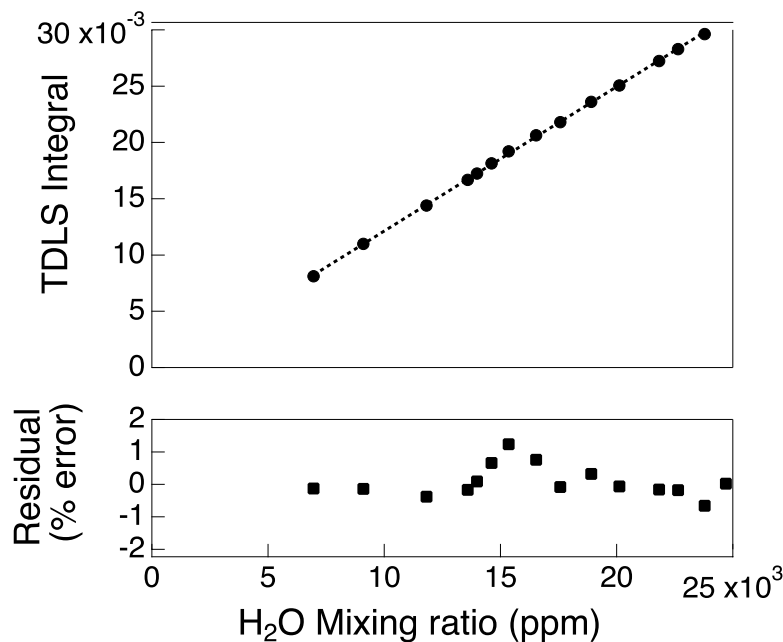
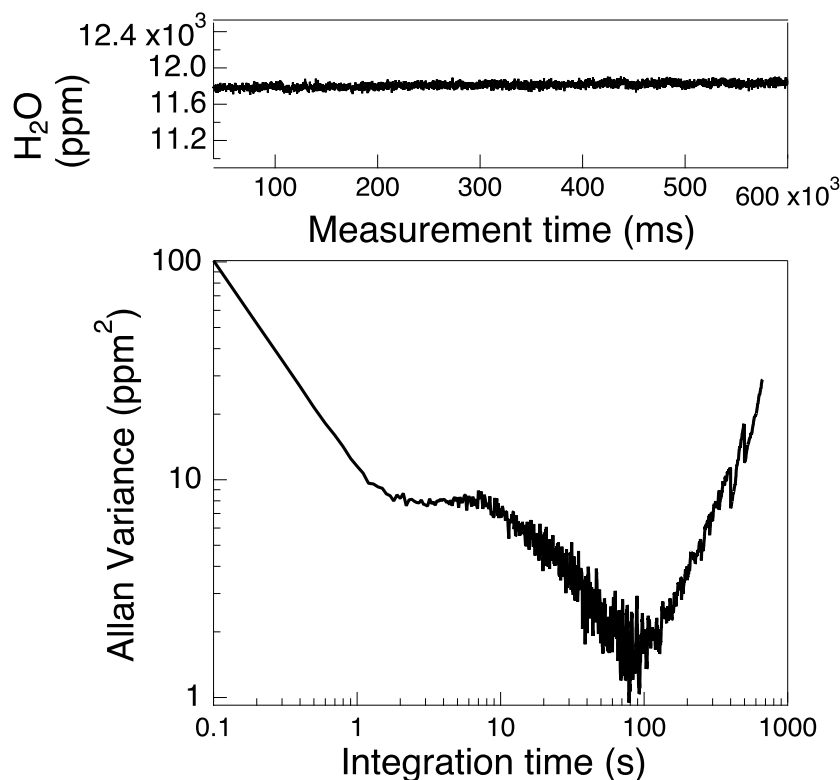


Figure 5. Top: Integral signal of the TDLs calculated as described in the text as a function of water vapor mixing ratio (black points). determined by simultaneous measurements with a Picarro L-2120i cavity ringdown spectrometer (e.g.,
210 Noone, et. al, 2008). The dashed line represents a linear fit to the results over the range 7,000 – 29,000 ppm. Bottom: Residual error, as percent of measurement, plotted for each of the points in the top panel.

The precision and stability of the TDLs were assessed using a standard Allan-Variance analysis (Werle et al., 1993). Precision is taken to be the square root of the Allan-Variance at the highest sample rate. To reduce variations in ambient water
215 vapor, the output fiber of the laser was attached to one end of the 53.3-cm long sample cell of the CU second-generation closed-path laser hygrometer (CLH-2) that was held at fixed pressure and temperature. The signal was detected with a InGaAs FC/APC-coupled detector (ThorLabs FGA04) as described elsewhere (Dorsi, et al., 2014). This detector is distinct from the ones previously described in this paper and it was used only for this experiment to couple the instrument to the sample cell. In this manner, electronic noise and drift could be assessed independent of variations in pressure, temperature, and water
220 concentration. An Allan-variance analysis of results, shown in Fig. 6, demonstrates a precision of 10 ppm at 0.1-s response time for a water abundance of 11,800 ppm. This represents a fractional absorbance of 10^{-3} for the conditions of the test. Averaging (increased integration time) allows the sensitivity to be improved by an order of magnitude down to 0.9 ppm at 34 s corresponding to a sensitivity of 1 in 10^{-4} .



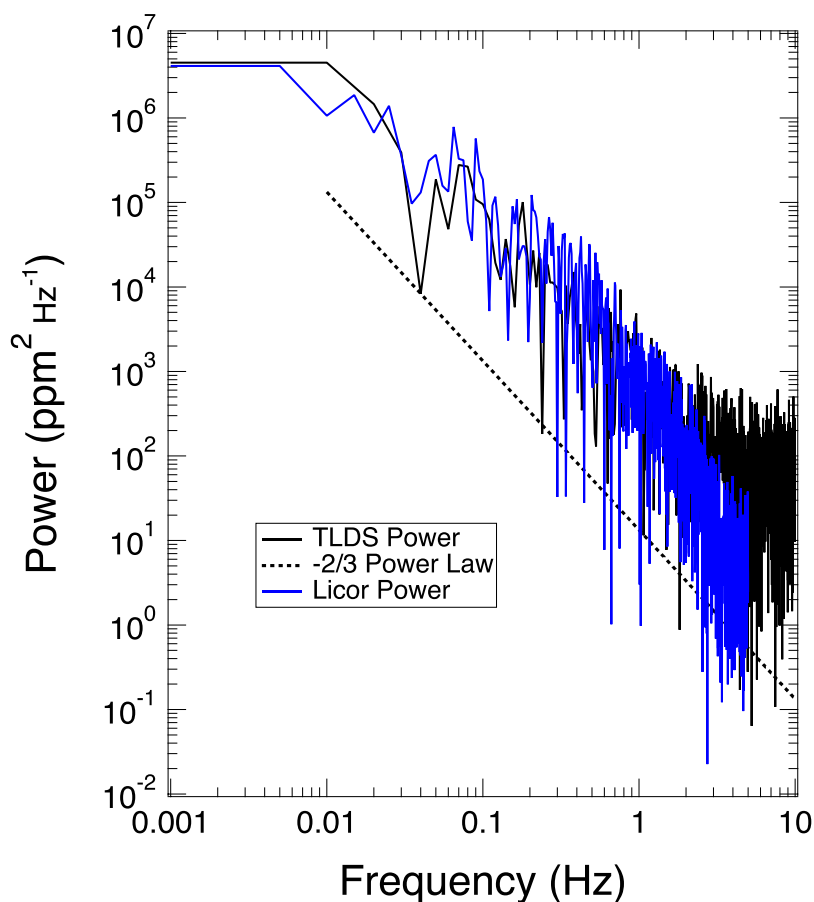
225 **Figure 6.** Top: Time series of water vapor mixing ratio for a 10-min segment from a laboratory measurement in a sealed
absorption cell held at constant temperature and pressure. Bottom: Allan variance calculated from segment of data displayed
in the top panel. The instrument demonstrates a precision of 10 ppm at 10 Hz (the intercept in the bottom panel).

The performance of the TDLS was assessed in several “real world” demonstrations, the goals of which were to
230 demonstrate stability for long-term observations and accurate quantification of fast variations of water vapor. The first
demonstration was an intercomparison with a commercial analyzer with a long history of eddy covariance measurements of
CO₂ and H₂O in a variety of environments (e.g. Burns et al., 2009; Ocheltree & Loescher, 2007; Pokorný et al., 2012; Zhao &
Tans, 2006). The LI-7000 (LiCor, Lincoln, NE) is a high-performance, dual-cell nondispersive infrared (NDIR) instrument
with an accuracy for H₂O of +/- 1% and a precision (RMS noise) of 2 ppm of at 5 Hz (LI-7000 CO₂/H₂O instruction manual;
235 Publication 984-07364, 2007). The site chosen for this test was the exterior of our laboratory where large variations in H₂O
would be expected from local sources such as vegetation and passing pedestrians. Figure 7 shows the power series densities
(PSD) for both instruments for a 1000-s segment of data.

At frequencies up to ~2 Hz the two instruments exhibit similar behavior, with power dropping with increasing
frequency following a $-2/3$ power law typical for long lived atmospheric variations (Wu et al., 2015). Above 2 Hz, the Li-
240 7000 power spectrum deviates below this power law due to damping of higher frequencies characteristic of closed-path



measurements (e.g., see Aslan et al., 2021). Conversely, the power spectrum of the TDLS trends above the power law at > 3 Hz, exhibiting a measurement precision of $\sim 10^{-3}$ absorbance, consistent with that determined from the Allan-variance analysis in the static cell, shown in Fig. 6.



245

Figure 7: Power spectral density (PSD) of the Li-7000 and new TDLS as a function of measurement frequency. The dotted line is the $-2/3$ power law that is expected for variability of ambient H_2O . The Li-7000 PSD does not extend beyond 5 Hz, the maximum sample rate of the instrument.

250 To test the long-term stability of the TLDS (e.g., days), we performed a three-day intercomparison with the same L2120-i CRDS used for calibrating the TDLS as described above. The TDLS and CRDS sampled from the top of a shipping container used for housing electronics in the Department of Atmospheric and Oceanic Sciences (ATOC) Skywatch Observatory located on East Campus (Lat 40.01° N 105.24° W, Elev: 1600 m) on the University of Colorado at Boulder. The CRDS sampled from a 3-m long, $\frac{1}{4}$ -in O.D. copper line running vertically up the side of the shipping container and terminating with a 3.8-cm radius,



255 180° bend to avoid ingesting precipitation. The optical cell for the TLDS was installed at the same elevation approximately
~1.5 m from this inlet. A long electrical line and A 25-m long fiber optic patch cable connected the output of the TDLS laser
to the collimating lens on the input of the optical cell, and a 10-m long twisted pair brought the detector signal back to the
TDLS electronics box which was housed in the shipping container. It is important to note that a better design would have
placed the detector amplifier close to the detector to reduce noise pick-up; therefore, this set-up likely represents “worst case”
260 noise of the TDLS for such a remote installation.

Observations from the TDLS and the CRDS instruments at their native resolutions of 10 Hz and 0.55 Hz, respectively,
are shown for three continuous days in Fig 8a. Over this period, H₂O mixing ratios varied from 5,000 ppm to 12,000 ppm, and
ambient temperature varied from 10.5 °C to 33.5 °C. There were multiple occurrences of precipitation and virga and periods
of variable cloud cover and direct sun. There were several important outcomes from this test. First, the detector/amplifier zero
265 signal from the TDLS (not shown here) varied from 0.006 V to 0.26 V (i.e., <10 % of average laser signal), from direct sunlight
or reflections, thus providing a good test of the validity of the method described above for extracting water vapor mixing ratios
from individual spectra. The background was successfully subtracted out before calculation, but this issue could be readily
addressed in a proper field experiment by suitable baffling of the optics to block the incoming solar radiation. Second, the
robustness and reliability of the spectroscopic foundation of the measurement was demonstrated by successful acquisition of
270 4.17 x 10⁶ unique and independent spectra over this period, with rejection of fewer than 0.05 % due to detector signal that was
clipped or filtered when the scan background used to calculate I₀ varied by more than 2 %. These losses of signal, which
typically lasted only a few seconds and self-corrected, occurred during precipitation on May 4th. They were likely due to
condensed water blocking the light path.

A scatterplot of the 3 days of continuous measurements from the TDLS and CRDS is shown in Fig. 8b. Over 5000
275 observations of 30-second averages are represented in this plot. The TDLS measurements were first averaged in bins of 20
measurements (e.g., to a 2-s time base) and the results then merged to the matching times recorded by the CDRS. Both
observations were then bin-averaged down to ~30 s to correspond with the digital smoothing inherent in the Picarro L-2120i
instruments. Despite being separated horizontally by ~1.5 m, the two instruments show remarkable agreement over the entire
sampling period, with < 4% deviation from a 1:1 correspondence and a 0.993 coefficient of determination (R²). It is noteworthy
280 that this averaging has removed 80 % of the variability of ambient H₂O largely due to what is occurring on the fastest
timescales.

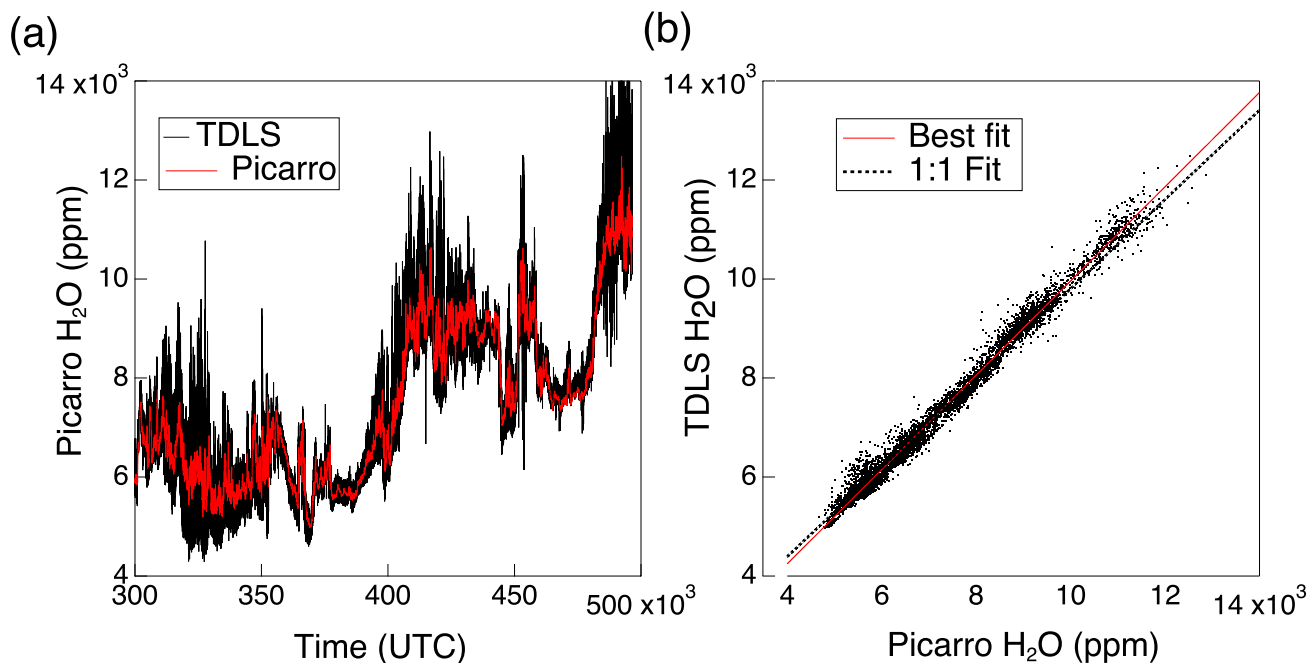


Figure 8: (a) Time series of Picarro and TDLS traces for a continuous sampling from 5-8 May 2023. UTC time 300,000 corresponds to 11:19 local time on 5 May. (b) Scatterplot of 30-s averages of measurements from the TDLS (y-axis) and
285 Picarro CRDS (x-axis).

Stability of the new TDLS was also assessed by examining three metrics of system performance, including detector signal at the start and end of each laser scan (representative of laser stability and optical efficiency), the ratio of these values (representative of laser and detector stability), and the position of the line center of the water vapor absorption feature (a direct
290 measure of temperature of the laser TEC). In all experiments described here, the ratio of amplified detector signal at the start and end of each scan was found to vary by less than 2 % after subtracting the zero-signal measured when the laser is powered off. In addition, the center position of the water vapor line drifted by +/- 1 scan index point or less from scan to scan. Based
295 on a calibration of the temperature dependence of line position using the setpoint of the PI controller to vary laser TEC temperature, it was found that this stability corresponds to < 0.001 K, a result that is consistent with the specifications of the WTC-3243.

4 Discussion

The goal of this work was to design, build, and characterize an economical and flexible fast-response instrument suitable for measurements of water vapor in the boundary layer. The entire electronics package is inexpensive and built with generalized components separated from the optical cell. A primary consideration was the use of low-cost, low power.



300 commercial off-the-shelf (COTS) components that, when combined with readily available lasers used by the telecom industry,
 allow for high-quality, high frequency observations at a fraction of the cost of commercial instruments with similar
 measurement characteristics. The key enabler for this new TDLS is the family of ARM-based microcontrollers based on the
 Cortex-M4 RISC integrated circuit. In this case, one controller is dedicated to controlling the laser in a highly reproducible
 manner required for maintaining tight temperature control with a commercial PI temperature controller package. In large part,
 305 the use of highly efficient microcontrollers resulted in a system that consumed only 2 W and could run for several hours on a
 pair of small, rechargeable batteries. The resulting total hardware cost of the instrument is mainly due to the laser, detector,
 and optics. The remaining components (Teensy's, board and various electronics) total ~\$300.

A list of components with manufacturer, model, mass, power consumption, and price at the time of purchase, is
 shown in Table 1:

310

Component	Part #	Mfc.	Mass (g)	Cost (\$)	Power (W)
Electronics Box			417	25	n/a
Custom printed circuit board		OSH Park	36	65	-
Distributed Feedback Laser	NLK1E56AA	NTT Innovative Devices		1700	0.325
Temperature controller	WTC 3243	Wavelength Electronics		100	0.50
Microcontrollers	Teensy (3.6 or 4.1)	PJRC		60	0.80
Power conditioning	misc	misc		20	0.40
Batteries	ARB-L16-700UP	Fenix		20	**
Detector amplifier circuit	misc	misc		15	0.025
Collimating lens, card cage, mounts		Thorlabs	916	300	n/a
InGaAs detector	FD1500	Fermionics		200	n/a
Total			1333	2500	2.05

Since this project was undertaken, the Teensy family of microcontrollers was impacted by global supply chain
 shortages of chips. Thus, the Teensy 3.6 is no longer available, and an alternative is needed to drive the laser. The primary
 consideration is that the laser driving function must be highly reproducible, both in ramp frequency and in power, to maintain
 315 precise tuning of the DFB output wavelength across the scan window. Replicating the measurements shown here would require
 generating ~1000 points per scan at a rate of 10 Hz (i.e., 10 kpsps), with 12-bit resolution and uniform time steps for each update
 of the DAC. Several microcontrollers have demonstrated this level of performance, including the ItsyBitsy M4 Express, which
 also employs the Cortex-M4 processor and fast 12-bit true analog DAC. It would also be straightforward to use the Teensy 4.1



digital lines to drive a commercial DAC chip such as the AD5638 series from Analog Devices. Also noteworthy, we have
320 carried out some tests showing that full scans over the water of ~ 1000 Hz are possible with the Teensy 3.6 and some of these
alternatives, potentially enabling high-accuracy sampling at 10-to-100-times the rates shown here, albeit with reduced precision.

Throughout the course of this work we experimented with other designs, including the components that convert the
voltage into current to drive the laser output, different configurations for the transimpedance amplifier, and lower voltage
electronics that allow for operation off a single 3.6 V lithium battery. In all cases similar high performance was maintained.
325 For example, we have successfully tested powered the laser with a miniature low-power diode laser driver (FL500, Wavelength
Electronics, Bozeman, MT). The FL500 also offers additional useful features such as overvoltage protection and enable/disable
pins to protect the laser. Out of convenience, all the results shown here were obtained with a simple transimpedance amplifier
circuit with the op-amp powered by 5 V, and with zero bias on the InGaAs detector. It is possible to further reduce
detector/amplifier noise by biasing the InGaAs detector with -2.5 V. Finally, we have successfully demonstrated that
330 significantly lower power consumption is possible by using components that operate at 3.3 V, thus eliminating the need for
two 3.6 V batteries in series.

One of the initial goals of this work was to develop a package that allows for quick swapping of lasers and optics in the
field. This is achieved by using a DFB laser in a standard butterfly package with integrated with TECs and fiber-coupled
FC/APC connector. Such an approach allows for swapping electronics with different lasers for probing different gases or for
335 swapping optical systems allowing for different optical path lengths required to achieve adequate sensitivity, including options
for employing folded optics such as Herriott Cells or retroreflectors. Future applications envisioned by our laboratory including
measurements of water vapor from stratospheric balloons, configuring for use on small unattended aerial vehicles, and
autonomous measurements from meteorological stations in remote locations, such as on buoys, the Antarctic plateau, or
mountain peaks.

340 **5 Conclusion**

We have developed an economical and flexible fast-response tunable diode laser spectrometer suitable for measurements of
water vapor in the atmospheric boundary layer (ABL). The instrument bridges the current gap between research grade
instruments costing tens of thousands of dollars and low-cost sensors commonly employed in portable meteorological stations
and hand-held devices. The novel feature of the new TDLS is the use of a pair of low-cost, low power microprocessors based
345 on the Cortex-M4 ARM family of integrated circuits. A series of intercomparisons with existing instruments used for high-
accuracy measurements of water vapor, including for eddy covariance, demonstrates that the new TDLS is well suited for
similar measurements for a fraction of the cost of existing instruments. Such a capability allows users with little previous
expertise in instrumentation to acquire high quality, fast-response observations of water vapor for a variety of applications,
including frequent horizontal and vertical profiling by uncrewed aerial vehicles, long-term eddy covariance measurements



350 from fixed and portable flux towers, and routine measurements of humidity from weather stations in remote locations such as
the polar ice caps, mountains, and glaciers.

Code availability: The extraction codes and Arduino sketches are available open source on GitHub.

355 *Data availability:* The data used in this paper are available from the corresponding author upon request.

Competing Interests: Some authors are members of the editorial board of journal AMT.

360 *Author Contributions:* DT conceived and managed the project, including acquiring funding. The new TDLS was designed
and fabricated by DT, EW, and LK. EW developed code for operating and extracting data from the TDLS. EW performed
experimental work and data analysis, with assistance from DT. Drafting of the manuscript was coordinated by EW with
contributions from all three authors.

Acknowledgements: We thank David Noone and Adriana Bailey for assistance with operation and maintenance of the Picarro
CRDS. We thank Scott Kittelman for access to the ATOC Skywatch Observatory and for technical support for field
measurements.

365 *Financial support:* Seed funding for this project was provided by the University of Colorado. Some material is based upon
work supported by the National Science Foundation under Grant No. AGS-2233136 and by the National Aeronautics and
Space Administration Earth Sciences Division, Award No. 80NSSC20K0729. Any opinions, findings, and conclusions or
recommendations expressed in this material are those of the authors and do not necessarily reflect the views of the National
Science Foundation, NASA, or the University of Colorado.

370

375

380



References

- LI-7000 CO₂ /H₂ O instruction manual, LICOR Biosciences. https://www.licor.com/env/pdf/gas_analyzers/7000/LI-7000Manual.pdf 984-07364, 22 October 2023.
- 385 Aslan, T., Peltola, O., Ibrom, A., Nemitz, E., Rannik, Ü., and Mammarella, I.: The high-frequency response correction of eddy covariance fluxes – Part 2: An experimental approach for analysing noisy measurements of small fluxes, *Atmos. Meas. Tech.*, 14, 5089–5106, <https://doi.org/10.5194/amt-14-5089-2021>, 2021.
- Aubinet, M., Vesala, T., and Papale, D. (Eds.): *Eddy Covariance: A Practical Guide to Measurement and Data Analysis*, Springer Netherlands, Dordrecht, <https://doi.org/10.1007/978-94-007-2351-1>, 2012.
- 390 Bärfuss, K. B., Schmithüsen, H., and Lampert, A.: Drone-based meteorological observations up to the tropopause – a concept study, *Atmos. Meas. Tech.*, 16, 3739–3765, <https://doi.org/10.5194/amt-16-3739-2023>, 2023.
- Burns, S. P., Delany, A. C., Sun, J., Stephens, B. B., Oncley, S. P., Maclean, G. D., Semmer, S. R., Schröter, J., and Ruppert, J.: An Evaluation of Calibration Techniques for In Situ Carbon Dioxide Measurements Using a Programmable Portable Trace-Gas Measuring System, *J. Atmos. Ocean. Tech.*, 26, 291–316, <https://doi.org/10.1175/2008JTECHA1080.1>, 2009.
- 395 Davis, S. M., Hallar, A. G., Avallone, L. M., and Engblom, W.: Measurement of Total Water with a Tunable Diode Laser Hygrometer: Inlet Analysis, Calibration Procedure, and Ice Water Content Determination, *J. Atmos. Ocean. Tech.*, 24, 463–475, <https://doi.org/10.1175/JTECH1975.1>, 2007.
- Dorsi, S. W., Kalnajs, L. E., Toohey, D. W., and Avallone, L. M.: A fiber-coupled laser hygrometer for airborne total water measurement, *Atmos. Meas. Tech.*, 7, 215–223, <https://doi.org/10.5194/amt-7-215-2014>, 2014.
- 400 Fabry, F.: The Spatial Variability of Moisture in the Boundary Layer and Its Effect on Convection Initiation: Project-Long Characterization, *Mon. Weather Rev.*, 134, 79–91, <https://doi.org/10.1175/MWR3055.1>, 2006.
- Fischer, L., Kiemle, C., and Craig, G. C.: Height-resolved variability of midlatitude tropospheric water vapor measured by an airborne lidar, *Geophys. Res. Lett.*, 39, L06803, <https://doi.org/10.1029/2011GL050621>, 2012.
- 405 Geerts, B., Raymond, D. J., Grubišić, V., Davis, C. A., Barth, M. C., Detwiler, A., Klein, P. M., Lee, W.-C., Markowski, P. M., Mullendore, G. L., and Moore, J. A.: Recommendations for In Situ and Remote Sensing Capabilities in Atmospheric Convection and Turbulence, *B. Am. Meteorol. Soc.*, 99, 2463–2470, <https://doi.org/10.1175/BAMS-D-17-0310.1>, 2018.
- Gordon, I. E., Rothman, L. S., Hargreaves, R. J., Hashemi, R., Karlovets, E. V., Skinner, F. M., Conway, E. K., Hill, C., Kochanov, R. V., Tan, Y., Wcisło, P., Finenko, A. A., Nelson, K., Bernath, P. F., Birk, M., Boudon, V., Campargue, A., Chance, K. V., Coustenis, A., Drouin, B. J., Flaud, J. –M., Gamache, R. R., Hodges, J. T., Jacquemart, D., Mlawer, E. J., Nikitin, A. V., Perevalov, V. I., Rotger, M., Tennyson, J., Toon, G. C., Tran, H., Tyuterev, V. G., Adkins, E. M., Baker, A., Barbe, A., Canè, E., Császár, A. G., Dudaryonok, A., Egorov, O., Fleisher, A. J., Fleurbaey, H., Foltynowicz, A., Furtenbacher, T., Harrison, J. J., Hartmann, J. –M., Horneman, V. –M., Huang, X., Karman, T., Karns, J., Kassi, S., Kleiner, I., Kofman, V., Kwabia-Tchana, F., Lavrentieva, N. N., Lee, T. J., Long, D. A., Lukashevskaya, A. A., Lyulin, O. M., Makhnev, V. Yu., Matt, W., Massie, S. T., Melosso, M., Mikhailenko, S. N., Mondelain, D., Müller, H. S. P., Naumenko, O. V., Perrin, A., Polyansky, O. L., Raddaoui, E., Raston, P. L., Reed, Z. D., Rey, M., Richard, C., Tóbiás, R., Sadiek, I., Schwenke, D. W., Starikova, E., Sung, K., Tamassia, F., Tashkun, S. A., Vander Auwera, J., Vasilenko, I. A., Viganin, A. A., Villanueva, G. L., Vispoel, B., Wagner, G., Yachmenev, A., and Yurchenko, S. N.: The HITRAN2020 molecular spectroscopic database, *J. Quant. Spectrosc. Ra.*, 277, 107949, <https://doi.org/10.1016/j.jqsrt.2021.107949>, 2022.
- 415



- 420 Hallar, A. G., Avallone, L. M., Herman, R. L., Anderson, B. E., and Heymsfield, A. J.: Measurements of ice water content in tropopause region Arctic cirrus during the SAGE III Ozone Loss and Validation Experiment (SOLVE), *J. Geophys. Res.*, 109, 2003JD004348, <https://doi.org/10.1029/2003JD004348>, 2004.
- 425 Helbig, M., Gerken, T., Beamesderfer, E. R., Baldocchi, D. D., Banerjee, T., Biraud, S. C., Brown, W. O. J., Brunzell, N. A., Burakowski, E. A., Burns, S. P., Butterworth, B. J., Chan, W. S., Davis, K. J., Desai, A. R., Fuentes, J. D., Hollinger, D. Y., Kljun, N., Mauder, M., Novick, K. A., Perkins, J. M., Rahn, D. A., Rey-Sanchez, C., Santanello, J. A., Scott, R. L., Seyednasrollah, B., Stoy, P. C., Sullivan, R. C., De Arellano, J. V.-G., Wharton, S., Yi, C., and Richardson, A. D.: Integrating continuous atmospheric boundary layer and tower-based flux measurements to advance understanding of land-atmosphere interactions, *Agr. Forest Meteorol.*, 307, 108509, <https://doi.org/10.1016/j.agrformet.2021.108509>, 2021.
- 430 Henze, D., Noone, D., and Toohey, D.: Detection of dilution due to turbulent mixing vs. precipitation scavenging effects on biomass burning aerosol concentrations using stable water isotope ratios during ORACLES, *Atmos. Chem. Phys.*, 23, 15269–15288, <https://doi.org/10.5194/acp-23-15269-2023>, 2023.
- Kämpfer, N. (Ed.): *Monitoring Atmospheric Water Vapour: Ground-Based Remote Sensing and In-situ Methods*, Springer New York, New York, NY, <https://doi.org/10.1007/978-1-4614-3909-7>, 2013.
- 435 Kiemle, C., Wirth, M., Fix, A., Rahm, S., Corsmeier, U., and Di Girolamo, P.: Latent heat flux measurements over complex terrain by airborne water vapour and wind lidars, *Q. J. Roy. Meteor. Soc.*, 137, 190–203, <https://doi.org/10.1002/qj.757>, 2011.
- Kim, D.-G., Bond-Lamberty, B., Ryu, Y., Seo, B., and Papale, D.: Ideas and perspectives: Enhancing research and monitoring of carbon pools and land-to-atmosphere greenhouse gases exchange in developing countries, *Biogeosciences*, 19, 1435–1450, <https://doi.org/10.5194/bg-19-1435-2022>, 2022.
- 440 Larson, V. E., Golaz, J.-C., and Cotton, W. R.: Small-Scale and Mesoscale Variability in Cloudy Boundary Layers: Joint Probability Density Functions, *J. Atmos. Sci.*, 59, 3519–3539, [https://doi.org/10.1175/1520-0469\(2002\)059<3519:SSAMVI>2.0.CO;2](https://doi.org/10.1175/1520-0469(2002)059<3519:SSAMVI>2.0.CO;2), 2002.
- Markwitz, C. and Siebicke, L.: Low-cost eddy covariance: a case study of evapotranspiration over agroforestry in Germany, *Atmos. Meas. Tech.*, 12, 4677–4696, <https://doi.org/10.5194/amt-12-4677-2019>, 2019.
- 445 May, R. D.: Open-path, near-infrared tunable diode laser spectrometer for atmospheric measurements of H₂O, *J. Geophys. Res.*, 103, 19161–19172, <https://doi.org/10.1029/98JD01678>, 1998.
- May, R. D. and Webster, C. R.: Data processing and calibration for tunable diode laser harmonic absorption spectrometers, *J. Quant. Spectrosc. Ra.*, 49, 335–347, [https://doi.org/10.1016/0022-4073\(93\)90098-3](https://doi.org/10.1016/0022-4073(93)90098-3), 1993.
- 450 Miloshevich, L. M., Paukkunen, A., Vömel, H., and Oltmans, S. J.: Development and Validation of a Time-Lag Correction for Vaisala Radiosonde Humidity Measurements, *J. Atmos. Oceanic Technol.*, 21, 1305–1327, [https://doi.org/10.1175/1520-0426\(2004\)021<1305:DAVOAT>2.0.CO;2](https://doi.org/10.1175/1520-0426(2004)021<1305:DAVOAT>2.0.CO;2), 2004.
- Miloshevich, L. M., Vömel, H., Whiteman, D. N., and Leblanc, T.: Accuracy assessment and correction of Vaisala RS92 radiosonde water vapor measurements, *J. Geophys. Res.*, 114, D11305, <https://doi.org/10.1029/2008JD011565>, 2009.
- 455 Muller, C. L., Chapman, L., Johnston, S., Kidd, C., Illingworth, S., Foody, G., Overeem, A., and Leigh, R. R.: Crowdsourcing for climate and atmospheric sciences: current status and future potential, *Int. J. Climatol.*, 35, 3185–3203, <https://doi.org/10.1002/joc.4210>, 2015.



- Newell, R. E., Zhu, Y., Browell, E. V., Ismail, S., Read, W. G., Waters, J. W., Kelly, K. K., and Liu, S. C.: Upper tropospheric water vapor and cirrus: Comparison of DC-8 observations, preliminary UARS microwave limb sounder measurements and meteorological analyses, *J. Geophys. Res.*, 101, 1931–1941, <https://doi.org/10.1029/95JD01373>, 1996.
- 460 Noone, D., Galewsky, J., Sharp, Z. D., Worden, J., Barnes, J., Baer, D., Bailey, A., Brown, D. P., Christensen, L., Crosson, E., Dong, F., Hurley, J. V., Johnson, L. R., Strong, M., Toohey, D., Van Pelt, A., and Wright, J. S.: Properties of air mass mixing and humidity in the subtropics from measurements of the D/H isotope ratio of water vapor at the Mauna Loa Observatory, *J. Geophys. Res.*, 116, D22113, <https://doi.org/10.1029/2011JD015773>, 2011.
- Ocheltree, T. W. and Loescher, H. W.: Design of the AmeriFlux Portable Eddy Covariance System and Uncertainty Analysis of Carbon Measurements, *J. Atmos. Ocean. Tech.*, 24, 1389–1406, <https://doi.org/10.1175/JTECH2064.1>, 2007.
- 465 Ogunjemiyo, S., Roberts, D. A., Keightley, K., Ustin, S. L., Hinckley, T., and Lamb, B.: Evaluating the relationship between AVIRIS water vapor and poplar plantation evapotranspiration, *J. Geophys. Res.*, 107, <https://doi.org/10.1029/2001JD001194>, 2002.
- Petersen, R. A.: On the Impact and Benefits of AMDAR Observations in Operational Forecasting—Part I: A Review of the Impact of Automated Aircraft Wind and Temperature Reports, *B. Am. Meteorol. Soc.*, 97, 585–602, <https://doi.org/10.1175/BAMS-D-14-00055.1>, 2016.
- 470 Pillar-Little, E. A., Greene, B. R., Lappin, F. M., Bell, T. M., Segales, A. R., De Azevedo, G. B. H., Doyle, W., Kanneganti, S. T., Tripp, D. D., and Chilson, P. B.: Observations of the thermodynamic and kinematic state of the atmospheric boundary layer over the San Luis Valley, CO, using the CopterSonde 2 remotely piloted aircraft system in support of the LAPSE-RATE field campaign, *Earth Syst. Sci. Data*, 13, 269–280, <https://doi.org/10.5194/essd-13-269-2021>, 2021.
- 475 Pokorný, R., Slípková, R., Havránková, K., and Pavelka, M.: ECOSYSTEM WATER USE EFFICIENCY OF NORWAY SPRUCE MONOCULTURE FROM EDDY-COVARIANCE AND ECOPHYSIOLOGICAL MEASUREMENTS, in: *ISHS Acta Horticulturae 951: VII International Symposium on Sap Flow*, Volterra, Italy, 1 June 2012, <https://doi.org/10.17660/ActaHortic.2012.951.36>, 2012.
- Rainwater, B. J.: *A New Approach for Ratiometric Measurements of Water Isotopologues*, University of Colorado Boulder, ISBN: 9798438790235, 2022.
- 480 Roth, H. A. and Blanken, P. D.: Controls and rates of evaporation from a water supply reservoir in the Colorado Front Range, *J. Hydrol.* 617, 129139, <https://doi.org/10.1016/j.jhydrol.2023.129139>, 2023.
- Santanello, J. A., Dirmeyer, P. A., Ferguson, C. R., Findell, K. L., Tawfik, A. B., Berg, A., Ek, M., Gentile, P., Guillod, B. P., Van Heerwaarden, C., Roundy, J., and Wulfmeyer, V.: Land–Atmosphere Interactions: The LoCo Perspective, *B. Am. Meteorol. Soc.*, 99, 1253–1272, <https://doi.org/10.1175/BAMS-D-17-0001.1>, 2018.
- 485 Segales, A. R., Greene, B. R., Bell, T. M., Doyle, W., Martin, J. J., Pillar-Little, E. A., and Chilson, P. B.: The CopterSonde: an insight into the development of a smart unmanned aircraft system for atmospheric boundary layer research, *Atmos. Meas. Tech.*, 13, 2833–2848, <https://doi.org/10.5194/amt-13-2833-2020>, 2020.
- 490 Segales, A. R., Chilson, P. B., and Salazar-Cerreño, J. L.: Considerations for improving data quality of thermo-hygrometer sensors on board unmanned aerial systems for planetary boundary layer research, *Atmos. Meas. Tech.*, 15, 2607–2621, <https://doi.org/10.5194/amt-15-2607-2022>, 2022.



- Shivers, S. W., Roberts, D. A., McFadden, J. P., and Tague, C.: An analysis of atmospheric water vapor variations over a complex agricultural region using airborne imaging spectrometry, *plos one*, 14, e0226014, <https://doi.org/10.1371/journal.pone.0226014>, 2019.
- 495 Trenberth, K. E., Fasullo, J., and Smith, L.: Trends and variability in column-integrated atmospheric water vapor, *Clim. Dynam.*, 24, 741–758, <https://doi.org/10.1007/s00382-005-0017-4>, 2005.
- Trent, T., Boesch, H., Somkuti, P., and Scott, N.: Observing Water Vapour in the Planetary Boundary Layer from the Short-Wave Infrared, *Remote Sens.-Basel*, 10, 1469, <https://doi.org/10.3390/rs10091469>, 2018.
- Varentsov, M., Konstantinov, P., Repina, I., Artamonov, A., Pechkin, A., Soromotin, A., Esau, I., and Baklanov, A.: Observations of the urban boundary layer in a cold climate city, *Urban Climate*, 47, 101351, <https://doi.org/10.1016/j.uclim.2022.101351>, 2023.
- 500 Werle, P., Mücke, R., and Slemr, F.: The limits of signal averaging in atmospheric trace-gas monitoring by tunable diode-laser absorption spectroscopy (TDLAS), *Appl. Phys. B*, 57, 131–139, <https://doi.org/10.1007/BF00425997>, 1993.
- 505 Wu, J. B., Zhou, X. Y., Wang, A. Z., and Yuan, F. H.: Comparative measurements of water vapor fluxes over a tall forest using open- and closed-path eddy covariance system, *Atmos. Meas. Tech.*, 8, 4123–4131, <https://doi.org/10.5194/amt-8-4123-2015>, 2015.
- Wulfmeyer, V., Hardesty, R. M., Turner, D. D., Behrendt, A., Cadetdu, M. P., Di Girolamo, P., Schlüssel, P., Van Baelen, J., and Zus, F.: A review of the remote sensing of lower tropospheric thermodynamic profiles and its indispensable role for the understanding and the simulation of water and energy cycles, *Rev. Geophys.* 53, 819–895, <https://doi.org/10.1002/2014RG000476>, 2015.
- 510 Zhao, C. L. and Tans, P. P.: Estimating uncertainty of the WMO mole fraction scale for carbon dioxide in air, *J. Geophys. Res.*, 111, 2005JD006003, <https://doi.org/10.1029/2005JD006003>, 2006.